RESEARCH ARTICLE | SEPTEMBER 16 2024

Barrier-crossing transition-path times for non-Markovian systems

L. Lavacchi ; R. R. Netz

J. Chem. Phys. 161, 114104 (2024)
https://doi.org/10.1063/5.0225742

The Journal of Chemical Physics ARTICLE pubs.aip.org/aip/jcp

Barrier-crossing transition-path times for non-Markovian systems

Cite as: J. Chem. Phys. 161, 114104 (2024); doi: 10.1063/5.0225742
Submitted: 26 June 2024 • Accepted: 28 August 2024 •
Published Online: 16 September 2024

L. Lavacchi[a] and R. R. Netz

AFFILIATIONS

Fachbereich Physik, Freie Universität Berlin, 14195 Berlin, Germany

[a]Author to whom correspondence should be addressed: lauraluna@zedat.fu-berlin.de

ABSTRACT

By simulation and asymptotic theory, we investigate the transition-path time of a one-dimensional finite-mass reaction coordinate crossing a double-well potential in the presence of non-Markovian friction. First, we consider single-exponential memory kernels and demonstrate that memory accelerates transition paths compared to the Markovian case, especially in the low-mass/high-friction limit. Then, we generalize to multi-exponential kernels and construct an asymptotic formula for the transition-path time that compares well with simulation data.

Many biological conformational transitions, particularly protein folding, can be modeled as diffusion in a one-dimensional free-energy landscape. While traditional ensemble-based experimental techniques have been extensively used to explore protein folding and unfolding kinetics, recently developed single-molecule experiments determined transition-path times in nucleic-acid and protein folding.[1–10] The measurement of transition-path times is challenging because transition paths, which correspond to the folding or unfolding trajectory segment when the system actually crosses over the barrier, are very short compared to the folding or unfolding time, as shown in Fig. 1. The potential barrier for protein folding or unfolding is typically higher than the characteristic thermal energy k_BT; for this reason, the protein spends most of the time in the folded or unfolded state. The experimental measurements of transition-path times, in turn, initiated novel theoretical and computational approaches.[11–18] Many of these studies considered Markovian models despite simulations and experimental studies suggesting that protein-folding dynamics is non-Markovian.[19–22] Accordingly, in the past years, several studies on the effects of non-Markovianity on transition paths have appeared.[20,23–25] The importance of memory for barrier crossing is shown in Fig. 1, where we plot simulation trajectories for two different memory times, for a relatively short memory time on the left and for a relatively long memory time on the right. In Figs. 1(a) and 1(b), we highlight the effect of memory on the first-passage time and show that a long memory time significantly increases the time that the system waits in the potential minimum before crossing the barrier. This memory-slowdown effect on the mean first-passage time occurs for long memory times, in fact, for intermediate memory times barrier-crossing acceleration is obtained, as has been discussed previously.[26–28] The corresponding transition paths in panels (c) and (d) demonstrate a more univocal effect of memory time on the transition-path time; it transpires that memory always induces a shortening of the transition-path time, even when the memory time is very long. While the effect of memory on barrier-crossing mean first-passage times is by now rather well understood, the effect of memory on transition-path times is less explored. In this paper, we also investigate the effect of inertia in combination with memory on the transition-path time, which is particularly relevant for proton-transfer processes that are characterized by low friction.[29,30]

We model the dynamics of a one-dimensional reaction coordinate by the generalized Langevin equation (GLE),[31–40]

$$m\ddot{x}(t) = -\int_{t_0}^{t} \Gamma(t-t')\dot{x}(t')dt' - \nabla U(x(t)) + F_R(t), \qquad (1)$$

where m is the effective mass, $\Gamma(t)$ the memory kernel, t_0 some initial time, and $\nabla U(x(t))$ denotes the gradient of a potential $U(x(t))$ that we take to be a double-well potential,

$$U(x) = U_0\left[\left(\frac{x}{L}\right)^2 - 1\right]^2, \qquad (2)$$

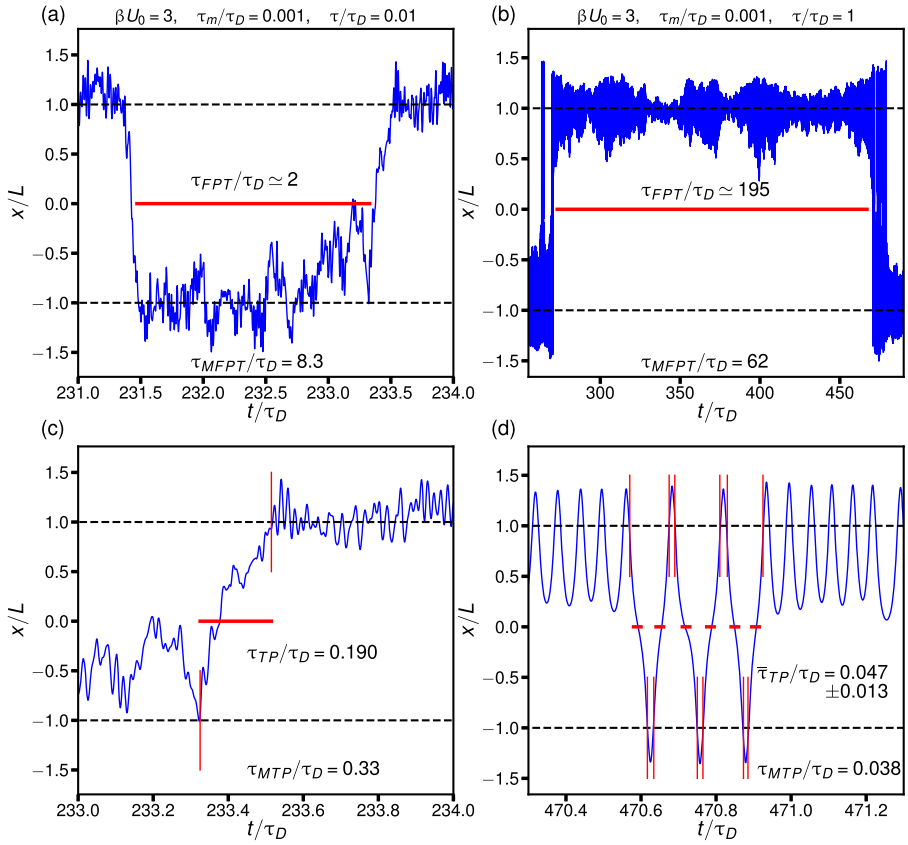

FIG. 1. Simulation trajectories of a non-Markovian barrier-crossing system for barrier height $\beta U_0 = 3$, rescaled inertial time $\tau_m/\tau_D = 0.001$ in panel (a), (c) short-memory limit with memory time $\tau/\tau_D = 0.01$, and in panel (b), (d) long-memory limit with memory time $\tau/\tau_D = 1$. The horizontal dashed black lines indicate the two potential minima. In panels (a) and (b), the horizontal red lines denote the first passage time τ_{FPT} and in panels (c) and (d), the transition-path time τ_{TP}. In panel (a), $\tau_{FPT}/\tau_D \simeq 2$, while the mean first-passage time is given by $\tau_{MFPT}/\tau_D = 8.3$, in panel (b), $\tau_{FPT}/\tau_D \simeq 195$ and $\tau_{MFPT}/\tau_D = 62$, and the mean first passage times (MFPT) are calculated by averaging over the entire trajectories. The vertical red lines in panels (c) and (d) highlight the last and the first time the reaction coordinate crosses a minimum before and after passing the barrier, respectively. In panel (c), the transition-path time is $\tau_{TP}/\tau_D = 0.190$, while the mean transition-path time obtained from the average over the entire trajectory is $\tau_{MTP}/\tau_D = 0.33$. In panel (d), $\bar{\tau}_{TP}/\tau_D = 0.047 \pm 0.013$ is the average over the six transition-path times shown in the figure, while $\tau_{MTP}/\tau_D = 0.038$ is the mean over the entire trajectory. The trajectories for long memory show pronounced oscillations in the minima and state-recrossings, meaning that the reaction coordinate immediately returns to the opposite minimum after reaching a minimum and thus resembles trajectories of high-inertial systems.[26,45,47]

with U_0 being the barrier height and L being the separation between the potential maximum and minima. $F_R(t)$ denotes the random force, characterized by a vanishing mean and the autocorrelation,

$$\begin{aligned} \langle F_R(t)\rangle &= 0, \\ \langle F_R(t)F_R(t')\rangle &= \beta^{-1}\Gamma(t-t'), \end{aligned} \tag{3}$$

where $\beta = 1/k_BT$. Equation (1) neglects nonlinear friction and is thus approximate[41–43] but has been demonstrated to be accurate for chemical-bond vibrations,[44] dihedral-angle dynamics,[45] protein folding,[21,22] and pair-reaction kinetics in water.[46] As a memory kernel, we choose in the first part of our paper, a single exponential,

$$\Gamma(t) = \frac{\gamma}{\tau} e^{-\frac{|t|}{\tau}}, \tag{4}$$

where τ is the memory time and γ is the friction coefficient. For the global discussion of the temporal scaling behavior, we introduce diffusion and inertial times, respectively, as

$$\begin{aligned} \tau_D &= \beta L^2 \gamma, \\ \tau_m &= \frac{m}{\gamma}. \end{aligned} \tag{5}$$

The diffusion time τ_D is the time it would take the reaction coordinate to diffuse by L in the overdamped Markovian limit and in the absence of a potential, the inertial time τ_m characterizes the time scale of viscous dissipation of momentum.

In a previous work,[16] it was shown for a Markovian system with finite mass and in the large-barrier limit, the mean transition-path time is given by

$$\tau_{MTP} = \frac{1}{\lambda_+(\gamma, m)} \left(\log(\beta U_0) + A(\gamma, m)\right), \tag{6}$$

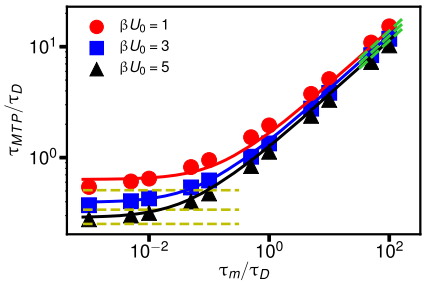

FIG. 2. Rescaled mean transition-path time τ_{MTP}/τ_D as a function of the rescaled inertial time τ_m/τ_D for various values of the rescaled barrier height βU_0 for a Markovian system ($\tau = 0$). The symbols represent the simulation data, and the lines represent Eq. (6). The dashed yellow horizontal lines and the green lines show the asymptotic behavior in the overdamped limit, Eq. (9), and in the inertial limit, Eq. (11).

where

$$\lambda_+(\gamma, m) = \frac{-\gamma + \sqrt{\Delta}}{2m}, \tag{7}$$

$$A(\gamma, m) = \log\left(\frac{4\sqrt{\Delta}}{\gamma + \sqrt{\Delta}} e^C\right), \tag{8}$$

with $\Delta = \gamma^2 + 8mU_0/L^2$ and $C = 0.577$ is the Euler–Mascheroni constant. This result was obtained by approximating the potential as a parabolic barrier.

In Fig. 2, we show the mean transition-path time τ_{MTP} as a function of the rescaled inertial time τ_m/τ_D and for various values of the potential height U_0 in the absence of memory effects, i.e., for $\tau = 0$. The colored lines show that Eq. (6) perfectly agrees with the simulation data plotted with different markers. Equation (6) was derived in the large barrier limit, but we observe that it well describes even the case when $\beta U_0 = 1$. The dashed yellow horizontal lines indicate the asymptotic result in the overdamped limit $\tau_m/\tau_D \to 0$, which is given by[13,16,17]

$$\tau^{\gamma}_{MTP} = \frac{\gamma L^2}{2U_0} \log(2e^C \beta U_0); \tag{9}$$

the derivation of Eq. (9) from Eq. (6) is shown in Appendix A.

In the inertial limit $\tau_D/\tau_m \to 0$, the mean transition-path time is given by[14]

$$\tau^{m}_{MTP} = \int_{U_0}^{\infty} dE \frac{\beta e^{-\beta E}}{e^{-\beta U_0}} \int_{-L}^{L} dx \sqrt{\frac{m/2}{E - U(x)}}. \tag{10}$$

If we approximate the double-well potential by a parabolic potential $U(x) = -U_0(x/L)^2$ around the barrier, we obtain in the high-barrier limit $\beta U_0 \gg 1$, the asymptotic expression,[12,16]

$$\tau^{m}_{MTP} \simeq \sqrt{\frac{m}{2U_0/L^2}} \log(4e^C \beta U_0); \tag{11}$$

the derivation is shown in Appendix B. The expression Eq. (11) is represented by the dashed green lines shown in Fig. 2 and agrees well with Eq. (6) in the inertial limit.

We now consider the effect of memory on τ_{MTP}, employing a harmonic approximation. For this, we first present analytical results for the positional autocorrelation function $C(t) = \langle x(t)x(0)\rangle$.[26,48] For the harmonic approximation of Eq. (1), we use $U(x) = Kx^2/2$, where K is the second derivative of the double-well potential at the minima, $K = U''(L) = 8U_0/L^2$. Fourier transforming Eq. (1) for $t_0 \to -\infty$ and solving for $\tilde{x}(\omega)$, we obtain

$$\tilde{x}(\omega) = \frac{\tilde{F}_R(\omega)}{K - m\omega^2 + i\omega\tilde{\Gamma}^+(\omega)} \equiv \tilde{\chi}(\omega)\tilde{F}_R(\omega), \tag{12}$$

which defines the response function $\tilde{\chi}(\omega)$. The half-sided Fourier transform $\tilde{\Gamma}^+(\omega)$ of $\Gamma(t)$ is given by

$$\tilde{\Gamma}^+ = \int_0^{\infty} dt e^{-i\omega t}\Gamma(t) = \frac{\gamma}{1 + i\omega\tau}, \tag{13}$$

while the Fourier transform of the symmetric random force correlation $\Gamma(t)$ is

$$\tilde{\Gamma}(\omega) = \tilde{\Gamma}^+(\omega) + \tilde{\Gamma}^+(-\omega) = \frac{2\gamma}{1 + \omega^2\tau^2}. \tag{14}$$

The Fourier transform of $C(t)$ is given by $\tilde{C}(\omega) = \beta^{-1}\tilde{\Gamma}(\omega)\tilde{\chi}(\omega)\tilde{\chi}(-\omega)$ and reads (see Appendix C)

$$\tilde{C}(\omega) = \frac{2\gamma\beta^{-1}(1 + \omega^2\tau^2)^{-1}}{\left(K - \omega^2\left[m - \frac{\tau\gamma}{1+\tau^2\omega^2}\right]\right)^2 + \frac{\omega^2\gamma^2}{(1+\omega^2\tau^2)^2}}. \tag{15}$$

This can be rewritten in a form that corresponds to the standard result for the memory-less (i.e., $\tau = 0$) harmonic oscillator,

$$\tilde{C}(\omega) = \frac{2\gamma_{\text{eff}}\beta^{-1}}{(K - m_{\text{eff}}\omega^2)^2 + \omega^2\gamma^2_{\text{eff}}}, \tag{16}$$

where we have introduced effective frequency-dependent expressions for the friction coefficient and the mass, according to

$$m_{\text{eff}} = m - c_1\tau\gamma_{\text{eff}}, \tag{17a}$$

$$\gamma_{\text{eff}} = \frac{\gamma}{1 + c_2\tau^2\omega^2}. \tag{17b}$$

It should be noted that the potential curvature K is not renormalized. In the expressions for m_{eff} and γ_{eff}, we have introduced two numerical constants that, in the harmonic case, take the values $c_1 = 1, c_2 = 1$ and will be used as heuristic parameters to account for non-harmonic corrections. From the expression for the effective friction, we see that γ_{eff} goes down as the memory time τ increases, which explains the quasi-inertial behavior shown in Figs. 1(b) and 1(d) for long memory times.[26] The poles of Eq. (16) in the low and high friction limits are obtained as $\omega_L^2 = K/m_{\text{eff}}$ for $Km_{\text{eff}} > \gamma^2_{\text{eff}}$ and $\omega_H^2 = -K^2/\gamma^2_{\text{eff}}$ for $Km_{\text{eff}} < \gamma^2_{\text{eff}}$, respectively. Using these characteristic frequencies, we obtain from Eq. (17b), the effective friction in the low-friction limit (see Appendix D),

$$\gamma^L_{\text{eff}} = \frac{\gamma}{1 + c_2\tau^2 K/m}, \tag{18}$$

while in the high-friction limit, we obtain Ref. 48 (see Appendix E),

$$\gamma_{\text{eff}}^{H} \simeq \gamma. \tag{19}$$

Inserting Eq. (18) into Eq. (17a) and rearranging such as to guarantee a positive effective mass, we obtain in the low-friction limit,

$$m_{\text{eff}}^{L} = \frac{m}{1 + c_1 \tau \gamma_{\text{eff}}^{L}/m}, \tag{20}$$

while in the high-friction limit, it follows that

$$m_{\text{eff}}^{H} = \frac{m}{1 + c_1 \tau \gamma/m}. \tag{21}$$

To obtain the mean transition-path time τ_{MTP} for finite memory time, we follow the approximate approach of a previous work[28] and use the effective parameters γ_{eff}^{L} and m_{eff}^{L} in the low friction limit, i.e., we insert the effective parameters (18) and (20) into Eq. (6) and arrive at the expression,

$$\tau_{MTP} = \frac{1}{\lambda_+(\gamma_{\text{eff}}^{L}, m_{\text{eff}}^{L})}\left(\log(\beta U_0) + A(\gamma_{\text{eff}}^{L}, m_{\text{eff}}^{L})\right). \tag{22}$$

Fitting the two constants to the simulation data, we obtain $c_1 = 0.1$ and $c_2 = 0.025$, as explained in Appendix F. Equation (6) was derived for transition paths that move over a barrier, i.e., for a harmonic potential with negative curvature,[16] while our effective parameters γ_{eff} and m_{eff} are calculated from the positional autocorrelation function in a harmonic potential, which is only well-defined for positive curvature. As demonstrated in Ref. 13, the transition-path time in a harmonic potential is perfectly continuous and well-behaved when crossing from negative to positive curvature. This analytic continuity justifies the combination of the two results for negative and positive curvatures; the relatively large deviations of the fitting parameters c_1 and c_2 from unity presumably stems from the fact that transition-path times are rather different in harmonic potentials with different signs of curvature.[13]

In Fig. 3, we show the mean transition-path time as a function of the rescaled memory time for various values of the rescaled inertial time and for fixed potential barrier height $\beta U_0 = 3$, a typical barrier height for protein-folding scenarios.[22,49] Equation (22), depicted by the colored lines, agrees well with the simulation data (symbols). In Ref. 23, the authors derived an expression for τ_{MTP} in the overdamped case for a power-law memory kernel, using the same procedure as in Ref. 16. They found that the transition-path time in the non-Markovian case is always smaller than in the Markovian case and monotonically decreases with increasing memory time. We also observe a monotonically decreasing τ_{MTP} with τ shown in Fig. 3, particularly for small masses and for intermediate memory times. It is also interesting to note that the mean first-passage time decreases with increasing memory time τ for intermediate values of τ, but that for long memory time, the mean first-passage time asymptotically increases as $\tau_{MFP} \sim \tau^2/\tau_D$[26] with τ. The mean first-passage time thus shows a behavior that is very different from the mean transition-path time.

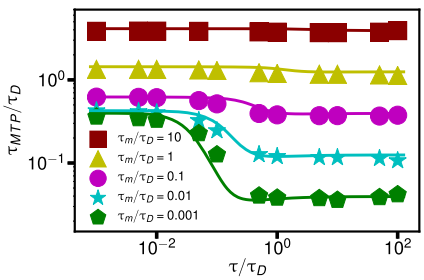

FIG. 3. Rescaled mean transition-path time τ_{MTP}/τ_D as a function of the rescaled memory time τ/τ_D for various values of the rescaled inertial time τ_m/τ_D and fixed potential height $\beta U_0 = 3$. The symbols represent the simulation data, and the lines represent Eq. (22).

We now study the scenario of a double exponential memory kernel, described by the kernel,

$$\Gamma(t) = \frac{\gamma_1}{\tau_1} e^{-\frac{|t|}{\tau_1}} + \frac{\gamma_2}{\tau_2} e^{-\frac{|t|}{\tau_2}}, \tag{23}$$

where we define $\gamma = \int_0^\infty \Gamma(t)dt = \gamma_1 + \gamma_2$ as the total friction coefficient. To obtain an explicit formula for the transition-path time with this more complex friction kernel, we sum the single-exponential formula Eq. (22) with frictional weights, according to

$$\tau_{MTP} = \frac{\gamma_1}{\gamma}\frac{1}{\lambda_+(\gamma_{\text{eff},1}^{L}, m_{\text{eff},1}^{L})}\left(\log(\beta U_0) + A(\gamma_{\text{eff},1}^{L}, m_{\text{eff},1}^{L})\right) + \frac{\gamma_2}{\gamma}\frac{1}{\lambda_+(\gamma_{\text{eff},2}^{L}, m_{\text{eff},2}^{L})}\left(\log(\beta U_0) + A(\gamma_{\text{eff},2}^{L}, m_{\text{eff},2}^{L})\right), \tag{24}$$

where the subscripts of the effective mass and effective friction coefficient denote which friction coefficient and memory time are considered. This form of the formula can be rationalized by drawing a parallel with the mean first-passage time for a multi-exponential friction kernel:[27,28] the MFPT has an overdamped and an energy-diffusion contribution. For a multi-exponential memory kernel, the overdamped term is additive in the exponential components, but the energy-diffusion term is inversely additive. For the transition-path time, there is no analog of an energy-diffusion contribution, and for this reason, we are left with a pure addition of the contributions for each term in the multi-exponential memory kernel. In Fig. 4, we compare Eq. (24) to simulation data as a function of γ_2/γ_1 for a rescaled inertial time $\tau_m/\tau_D = 0.01$, potential barrier height $\beta U_0 = 3$, and fixed memory time $\tau_2/\tau_D = 31.6$ for various values of τ_1/τ_D. We choose a relatively small inertial time because in the inertial limit, the transition-path time becomes almost independent of the memory time, as shown in Fig. 3. The agreement between the simulation data and Eq. (24) shown in Fig. 4 is good, in particular for $\tau_1/\tau_D = 0.0316$ and $\tau_1/\tau_D = 0.316$, since for these memory-time values, the transition-path time is rather constant, as shown in Fig. 3. For the intermediate value of $\tau_1/\tau_D = 0.1$, one notices some disagreement between the simulation data and Eq. (24), which we rationalize by the fact that around $\tau/\tau_D = 0.1$, the transition-path time simulation data shown in Fig. 3 vary significantly with τ/τ_D in a fashion that is not perfectly matched by the formula Eq. (22). We also note

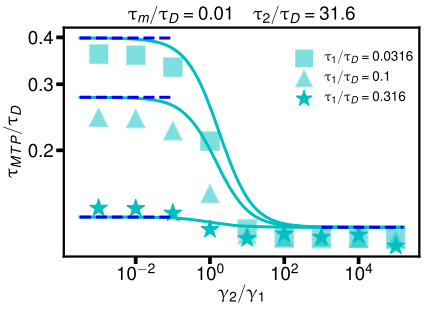

FIG. 4. Mean transition-path time for a double-exponential memory kernel as a function of the ratio between the two friction coefficients γ_2/γ_1 for fixed inertial time $\tau_m/\tau_D = 0.01$, memory time $\tau_2/\tau_D = 31.6$, and potential barrier height $\beta U_0 = 3$ for various values of τ_1/τ_D. The symbols represent the simulation data, and the lines represent Eq. (24). The horizontal blue dashed lines denote predictions according to the single-exponential formula in Eq. (22) based on τ_1/τ_D to the left-hand side and based on τ_2/τ_D to the right-hand side.

that the scaling of the vertical axis shown in Fig. 4 is smaller than that shown in Fig. 3, which increases deviations.

The generalization of Eq. (24) to a memory kernel consisting of N exponentials is straightforward and reads

$$\tau_{MTP} = \sum_{i=1}^{N} \frac{\gamma_i}{\gamma} \frac{1}{\lambda_+(\gamma^L_{\mathrm{eff,i}}, m^L_{\mathrm{eff,i}})} \left(\log(\beta U_0) + A(\gamma^L_{\mathrm{eff,i}}, m^L_{\mathrm{eff,i}})\right), \quad (25)$$

which is an explicit formula for the mean transition-path time of a reaction over a barrier for general multi-exponential memory in the presence of inertial effects.

In conclusion, starting from the GLE, we derived an asymptotic formula for the mean transition-path time in the presence of a single-exponential memory function using the previously derived expression, Eq. (6), in the Markovian limit.[16] Our approach is based on asymptotic expressions for the effective mass and effective friction coefficient in the harmonic approximation that account for non-Markovian effects.[48] The asymptotic result in Eq. (22) agrees perfectly with the simulation data and shows that the mean transition-path time decreases monotonically with increasing memory time. The transition-path time saturates for small and large memory times and varies only in a rather narrow range of intermediate memory-time values where the memory time is comparable with the diffusion time scale; the influence of memory on the mean transition-path time is most dramatic for small mass or high friction. We also investigate the double-exponential memory kernel scenario, where the additive expression Eq. (24) describes the simulation data quite well. Based on these results, we propose an explicit formula in Eq. (25) for the mean transition-path time in the presence of a general multi-exponential memory function. Together with our previously derived asymptotic formulas for the mean first-passage time for finite mass and multi-exponential friction kernel,[27,28] we thus have a general description of the reaction kinetics of non-Markovian systems in terms of their mean first passage or waiting times and their mean transition-path times.

We acknowledge support from the Deutsche Forschungsgemeinschaft Grant No. CRC 1114, Project No. 235221301-B03, by the ERC Advanced Grant No. 835117 NoMaMemo, and by the Infosys Foundation.

AUTHOR DECLARATIONS

Conflict of Interest

The authors have no conflicts to disclose.

Author Contributions

L. Lavacchi: Conceptualization (equal); Formal analysis (equal). **R. R. Netz**: Supervision (equal); Writing – review & editing (equal).

DATA AVAILABILITY

The data that support the findings of this study are available from the corresponding author upon reasonable request.

APPENDIX A: TRANSITION-PATH TIME IN THE OVERDAMPED LIMIT

In the overdamped limit, we have $\Delta = \gamma^2 + 4mK_{\mathrm{bar}} = \gamma^2 + 8mU_0/L^2 \simeq \gamma^2$, where $K_{\mathrm{bar}} = 2U_0/L^2$ is the magnitude of the potential curvature at the top. By inserting this value for Δ into Eq. (8), we obtain

$$A = \log\left(\frac{4\sqrt{\Delta}}{\gamma+\sqrt{\Delta}} e^C\right) \simeq \log\left(\frac{4\gamma}{2\gamma} e^C\right) = \log\left(2e^C\right). \quad (A1)$$

For λ_+, we obtain

$$\begin{aligned}\lambda_+ &= \frac{-\gamma + \sqrt{\gamma^2 + 4mK_{\mathrm{bar}}}}{2m} \\ &= \frac{-\gamma + \sqrt{\gamma^2(1 + 8m\ U_0/\gamma^2L^2)}}{2m} \\ &\simeq \frac{\gamma(-1+1+4mU_0/\gamma^2L^2)}{2m} = 2U_0/\gamma L^2. \end{aligned} \quad (A2)$$

Inserting these limiting values into Eq. (6), we arrive at Eq. (9), which agrees with the asymptotic result in Ref. 16.

APPENDIX B: TRANSITION-PATH TIME IN THE INERTIAL LIMIT

The mean transition-path time follows from the transition-path time distribution as

$$\tau_{MTP} = \int_0^\infty dt\ p_{TP}(t)\ t. \quad (B1)$$

In the inertial limit, the transition-path time is a function of the total energy and given by

$$\tau_{TP}(E) = \int_{-L}^{L} \frac{dx\sqrt{m/2}}{\sqrt{E-U(x)}}. \quad (B2)$$

In the canonical ensemble, the distribution of transition-path times is given by

$$p_{TP}(t) = \frac{\int_{U_0}^{\infty} dE\, e^{-\beta E}\delta(t-\tau_{TP}(E))}{\int_{U_0}^{\infty} dE\, e^{-\beta E}}. \tag{B3}$$

For a parabolic barrier, the distribution can be rewritten as

$$p_{TP}(t) = \sqrt{\frac{2\beta U_0}{m}}\beta U_0 \frac{\cosh\left(\sqrt{\frac{2\beta U_0}{m}}t/2\right)}{\sinh^3\left(\sqrt{\frac{2\beta U_0}{m}}t/2\right)} \times \exp\left[-\frac{\beta U_0}{\sinh^2\left(\sqrt{\frac{2\beta U_0}{m}}t/2\right)}\right], \tag{B4}$$

which in the limit of high barrier $\beta U_0 \gg 1$ becomes

$$p_{TP}(t) \approx 4\sqrt{\frac{2\beta U_0}{m}}\beta U_0 \exp\left[-\sqrt{\frac{2\beta U_0}{m}}t - 4\beta U_0 e^{-\sqrt{\frac{2\beta U_0}{m}}t}\right]. \tag{B5}$$

The maximum of the distribution is obtained for $t = \sqrt{\frac{m}{2\beta U_0}}\ln(4\beta U_0)$, and the corresponding mean transition-path time is given by Eq. (11).

APPENDIX C: DERIVATION OF THE FOURIER TRANSFORM OF THE POSITION AUTOCORRELATION FUNCTION

Using the Fourier transform of the generalized Langevin equation,

$$\tilde{x}(\omega) = \frac{\tilde{F}_R(\omega)}{K - m\omega^2 + i\omega\tilde{\Gamma}_V^+(\omega)} \equiv \tilde{\chi}(\omega)\tilde{F}_R(\omega), \tag{C1}$$

we can write the autocorrelation function as

$$\begin{aligned} C(t) \equiv \langle x(t)x(0)\rangle &= \int\frac{d\omega}{2\pi}e^{i\omega t}\int\frac{d\omega'}{2\pi}\langle\tilde{x}(\omega)\tilde{x}(\omega')\rangle \\ &= \int\frac{d\omega}{2\pi}e^{i\omega t}\int\frac{d\omega'}{2\pi}\tilde{\chi}(\omega)\tilde{\chi}(\omega')\langle\tilde{F}_R(\omega)\tilde{F}_R(\omega')\rangle \\ &= k_BT\int\frac{d\omega}{2\pi}e^{i\omega t}\int\frac{d\omega'}{2\pi}2\pi\delta(\omega+\omega')\tilde{\Gamma}_R(\omega)\tilde{\chi}(\omega)\tilde{\chi}(\omega') \\ &= k_BT\int\frac{d\omega}{2\pi}e^{i\omega t}\tilde{\Gamma}_R(\omega)\tilde{\chi}(\omega)\tilde{\chi}(-\omega), \end{aligned} \tag{C2}$$

where we used $\langle\tilde{F}_R(\omega)\tilde{F}_R(\omega')\rangle = k_BT2\pi\delta(\omega+\omega')\tilde{\Gamma}_R(\omega)$. From this, the Fourier transform of the autocorrelation function follows as

$$\tilde{C}(\omega) = \beta^{-1}\tilde{\Gamma}_R(\omega)\tilde{\chi}(\omega)\tilde{\chi}(-\omega). \tag{C3}$$

APPENDIX D: LOW-FRICTION LIMIT

In low-friction limit, Eq. (16) is dominated by the pole,

$$\omega_L^2 = K/m_{\text{eff}} \quad \text{for} \quad \frac{Km_{\text{eff}}}{\gamma_{\text{eff}}^2} > 1. \tag{D1}$$

Inserting Eq. (D1) into Eq. (17b), we arrive at a quadratic equation,

$$\begin{aligned} \gamma_{\text{eff}} &= \frac{\gamma}{1+\frac{c_2\tau^2K}{m-c_1\tau\gamma_{\text{eff}}}}, \\ \gamma_{\text{eff}}(m - c_1\tau\gamma_{\text{eff}} + c_2\tau^2K) &= \gamma(m - c_1\tau\gamma_{\text{eff}}), \\ \gamma_{\text{eff}}^2 - \gamma_{\text{eff}}\left(\frac{m}{c_1\tau} + \frac{c_2}{c_1}\tau K + \gamma\right) + \frac{\gamma m}{c_1\tau} &= 0, \\ \gamma_{\text{eff}} = \frac{m}{2c_1\tau} + \frac{c_2\tau K}{2c_1} + \frac{\gamma}{2} &\pm \sqrt{\left(\frac{m}{2c_1\tau} + \frac{c_2\tau K}{2c_1} + \frac{\gamma}{2}\right)^2 - \frac{\gamma m}{c_1\tau}}, \\ \gamma_{\text{eff}} = \frac{m}{2c_1\tau} + \frac{c_2\tau K}{2c_1} + \frac{\gamma}{2} &\pm \sqrt{\left(\frac{m}{2c_1\tau} + \frac{c_2\tau K}{2c_1} - \frac{\gamma}{2}\right)^2 + \frac{c_2}{c_1}\tau K\gamma}. \end{aligned}$$

For small τ, we obtain

$$\gamma_{\text{eff}} = \frac{m}{2c_1\tau} + \frac{c_2\tau K}{2c_1} + \frac{\gamma}{2} \pm \frac{m}{2c_1\tau}\left[\left(1 + c_2\frac{\tau^2K}{m} - \frac{c_1\tau\gamma}{m}\right)^2 + \frac{4c_1c_2\tau^3K\gamma}{m^2}\right]^{1/2}$$

$$\gamma_{\text{eff}} \simeq \frac{m}{2c_1\tau} + \frac{c_2\tau K}{2c_1} + \frac{\gamma}{2} \pm \frac{m}{2c_1\tau}\left[1 - \frac{2c_1\tau\gamma}{m} + \frac{2c_2\tau^2K}{m} + \frac{c_1^2\tau^2\gamma^2}{m^2} + \frac{2c_1c_2\tau^3K\gamma}{m^2}\right]^{1/2}$$

$$\gamma_{\text{eff}} \simeq \frac{m}{2c_1\tau} + \frac{c_2\tau K}{2c_1} + \frac{\gamma}{2} \pm \frac{m}{2c_1\tau}\left(1 - \frac{c_1\tau\gamma}{m} + \frac{c_2\tau^2K}{m} + \frac{2c_1c_2\tau^3K\gamma}{m^2}\right)$$

and taking the minus sign,

$$\Rightarrow \gamma_{\text{eff}} \simeq \gamma - \gamma\frac{c_2\tau^2K}{m}. \tag{D2}$$

For large τ, we obtain

$$\gamma_{\rm eff} = \frac{m}{2c_1\tau} + \frac{c_2\tau K}{2c_1} + \frac{\gamma}{2} \pm \frac{c_2\tau K}{2c_1}\left[\left(1 + \frac{c_1\gamma}{c_2\tau K} + \frac{m}{c_2\tau^2 K}\right)^2 - \frac{4c_1\gamma m}{c_2^2\tau^3K^2}\right]^{1/2}$$

$$\gamma_{\rm eff} \simeq \frac{m}{2c_1\tau} + \frac{c_2\tau K}{2c_1} + \frac{\gamma}{2} \pm \frac{c_2\tau K}{2c_1}\left[1 + \frac{2c_1\gamma}{c_2\tau K} + \frac{2m}{c_2\tau^2 K} + \frac{c_1^2\gamma^2}{c_2^2\tau^2K^2} + \frac{2c_1\gamma m}{c_2^2\tau^3K^2} - \frac{4c_1\gamma m}{c_2^2\tau^3K^2}\right]^{1/2}$$

$$\gamma_{\rm eff} \simeq \frac{m}{2c_1\tau} + \frac{c_2\tau K}{2c_1} + \frac{\gamma}{2} \pm \frac{c_2\tau K}{2c_1}\left[1 + \frac{2c_1\gamma}{c_2\tau K} + \frac{2m}{c_2\tau^2 K} + \frac{c_1^2\gamma^2}{c_2^2\tau^2K^2} - \frac{2c_1\gamma m}{c_2^2\tau^3K^2}\right]^{1/2}$$

$$\gamma_{\rm eff} \simeq \frac{m}{2c_1\tau} + \frac{c_2\tau K}{2c_1} + \frac{\gamma}{2} \pm \frac{c_2\tau K}{2c_1}\left(1 + \frac{c_1\gamma}{c_2\tau K} + \frac{m}{c_2\tau^2 K} - \frac{2c_1\gamma m}{c_2^2\tau^3K^2}\right)$$

and taking the minus sign,

$$\Rightarrow \gamma_{\rm eff} \simeq \frac{\gamma m}{c_2\tau^2 K}. \tag{D3}$$

Combining the two limits Eqs. (D2) and (D3), we obtain the expression,

$$\gamma_{\rm eff}^L = \frac{\gamma}{1 + \frac{c_2\tau^2 K}{m}}. \tag{D4}$$

Inserting Eq. (D4) into Eq. (17a), we obtain the expression,

$$m_{\rm eff}^L = m - \frac{c_1\tau\gamma}{1 + c_2\tau^2 K/m}. \tag{D5}$$

APPENDIX E: HIGH-FRICTION LIMIT

In the high-friction limit, Eq. (16) is dominated by the pole,

$$\omega_H^2 = -K^2/\gamma_{\rm eff}^2 \quad \frac{Km_{\rm eff}}{\gamma_{\rm eff}^2} < 1. \tag{E1}$$

Inserting this expression into Eq. (17b), we obtain

$$\gamma_{\rm eff} = \frac{\gamma}{1 - \tau^2K^2/\gamma_{\rm eff}^2} = \frac{\gamma\gamma_{\rm eff}^2}{\gamma_{\rm eff}^2 - \tau^2K^2},$$

$$\gamma_{\rm eff}^2 - \gamma\gamma_{\rm eff} - \tau^2K^2 = 0,$$

$$\gamma_{\rm eff} = \frac{\gamma}{2} \pm \sqrt{\frac{\gamma^2}{4} + \tau^2K^2},$$

and taking the positive sign,

$$\Rightarrow \gamma_{\rm eff}^H = \frac{\gamma}{2}\left[1 + \left(1 + \frac{4\tau^2K^2}{\gamma^2}\right)^{1/2}\right] \simeq \gamma.$$

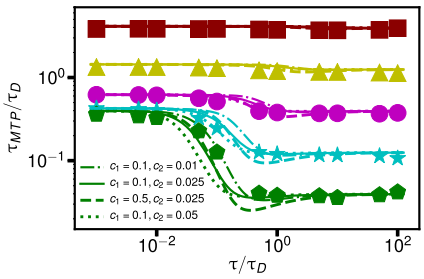

FIG. 5. Rescaled mean transition-path time τ_{MTP}/τ_D as a function of the rescaled memory time τ/τ_D for various values of the rescaled inertial time τ_m/τ_D as shown in Fig. 3 and fixed barrier height $\beta U_0 = 3$. The symbols represent the simulation data, and the lines represent Eq. (22) for different values of the constants c_1 and c_2, as given in the legend.

APPENDIX F: FIT PROCEDURE FOR OBTAINING c_1 AND c_2

In Fig. 5, we show the same simulation data as in Fig. 3 and compare to Eq. (22) for different values of the two constants c_1 and c_2. The values $c_1 = 0.1, c_2 = 0.025$ lead to the best overall agreement with the simulation data. The dotted–dashed line for the values $c_1 = 0.1$, $c_2 = 0.01$ describes the simulation data well for low mass but is off for high mass $\tau_m/\tau_D = 0.01$ and $\tau_m/\tau_D = 0.1$.

REFERENCES

[1] P. Hänggi, P. Talkner, and M. Borkovec, "Reaction-rate theory: Fifty years after Kramers," Rev. Mod. Phys. **62**, 251 (1990).
[2] H. S. Chung, J. M. Louis, and W. A. Eaton, "Experimental determination of upper bound for transition path times in protein folding from single-molecule photon-by-photon trajectories," Proc. Natl. Acad. Sci. U. S. A. **106**, 11837 (2009).
[3] K. Neupane, D. B. Ritchie, H. Yu, D. A. N. Foster, F. Wang, and M. T. Woodside, "Transition path times for nucleic acid folding determined from energy-landscape analysis of single-molecule trajectories," Phys. Rev. Lett. **109**, 068102 (2012).
[4] H. S. Chung, J. M. Louis, and W. A. Eaton, "Single-molecule fluorescence experiments determine protein folding transition path times," Science **335**, 981 (2012).
[5] K. Truex, H. S. Chung, J. M. Louis, and W. A. Eaton, "Testing landscape theory for biomolecular processes with single molecule fluorescence spectroscopy," Phys. Rev. Lett. **115**, 018101 (2015).
[6] K. Neupane, D. A. N. Foster, D. R. Dee, H. Yu, F. Wang, and M. T. Woodside, "Direct observation of transition paths during the folding of proteins and nucleic acids," Science **352**, 239 (2016).

[7]K. Neupane, F. Wang, and M. T. Woodside, "Direct measurement of sequence-dependent transition path times and conformational diffusion in DNA duplex formation," Proc. Natl. Acad. Sci. U. S. A. **114**, 1329 (2017).
[8]N. Q. Hoffer, K. Neupane, A. G. T. Pyo, and M. T. Woodside, "Measuring the average shape of transition paths during the folding of a single biological molecule," Proc. Natl. Acad. Sci. U. S. A. **116**, 8125 (2019).
[9]N. Q. Hoffer and M. T. Woodside, "Probing microscopic conformational dynamics in folding reactions by measuring transition paths," Curr. Opin. Chem. Biol. **53**, 68 (2019).
[10]J.-Y. Kim and H. S. Chung, "Disordered proteins follow diverse transition paths as they fold and bind to a partner," Science **368**, 1253 (2020).
[11]G. Hummer, "From transition paths to transition states and rate coefficients," J. Chem. Phys. **120**, 516 (2004).
[12]S. Chaudhury and D. E. Makarov, "A harmonic transition state approximation for the duration of reactive events in complex molecular rearrangements," J. Chem. Phys. **133**, 034118 (2010).
[13]W. K. Kim and R. R. Netz, "The mean shape of transition and first-passage paths," J. Chem. Phys. **143**, 143 (2015).
[14]J. O. Daldrop, W. K. Kim, and R. R. Netz, "Transition paths are hot," Europhys. Lett. **113**, 18004 (2016).
[15]E. Pollak, "Transition path time distribution and the transition path free energy barrier," Phys. Chem. Chem. Phys. **18**, 28872 (2016).
[16]M. Laleman, E. Carlon, and H. Orland, "Transition path time distributions," J. Chem. Phys. **147**, 214103 (2017).
[17]P. Cossio, G. Hummer, and A. Szabo, "Transition paths in single-molecule force spectroscopy," J. Chem. Phys. **148**, 123309 (2018).
[18]R. S. A. M. Berezhkovskii and D. E. Makarov, "Broad distributions of transition-path times are fingerprints of multidimensionality of the underlying free energy landscapes," Proc. Natl. Acad. Sci. U. S. A. **117**, 27116 (2022).
[19]S. V. Krivov, "Is protein folding sub-diffusive?," PLoS Comput. Biol. **6**, 1000921 (2010).
[20]R. Satija, A. Das, and D. E. Makarov, "Transition path times reveal memory effects and anomalous diffusion in the dynamics of protein folding," J. Chem. Phys. **147**, 147 (2017).
[21]C. Ayaz, L. Trepper, F. N. Brünig, J. Kappler, Jr., O. Daldrop, and R. R. Netz, "Non-Markovian modeling of protein folding," Proc. Natl. Acad. Sci. U. S. A. **118**, e2023856118 (2021).
[22]B. A. Dalton, C. Ayaz, H. Kiefer, A. Klimek *et al.*, "Fast protein folding is governed by memory-dependent friction," Proc. Natl. Acad. Sci. U. S. A. **120**, e2220068120 (2023).
[23]E. Carlon, H. Orland, T. Sakaue, and C. Vanderzande, "Effect of memory and active forces on transition path time distributions," J. Phys. Chem. B **122**, 11186 (2018).
[24]R. Satija and D. E. Makarov, "Generalized Langevin equation as a model for barrier crossing dynamics in biomolecular folding," J. Phys. Chem. B **123**, 802 (2019).
[25]D. Singh, K. Mondal, and S. Chaudhury, "Effect of memory and inertial contribution on transition-time distributions: Theory and simulations," J. Phys. Chem. B **125**, 4536 (2021).
[26]J. Kappler, J. O. Daldrop, F. N. Brünig, M. D. Boehle, and R. R. Netz, "Memory-induced acceleration and slowdown of barrier crossing," J. Chem. Phys. **148**, 014903 (2018).
[27]J. Kappler, V. B. Hinrichsen, and R. R. Netz, "Non-Markovian barrier crossing with two-time-scale memory is dominated by the faster memory component," Eur. Phys. J. E **42**, 119 (2019).
[28]L. Lavacchi, J. Kappler, and R. R. Netz, "Barrier crossing in the presence of multi-exponential memory functions with unequal friction amplitudes and memory times," Europhys. Lett. **131**, 40004 (2020).
[29]F. N. Brünig, M. Rammler, E. M. Adams, M. Havenith, and R. R. Netz, "Spectral signatures of excess-proton waiting and transfer-path dynamics in aqueous hydrochloric acid solutions," Nat. Commun. **13**, 4210 (2022).
[30]F. N. Brünig, P. Hillmann, W. K. Kim, J. O. Daldrop, and R. R. Netz, "Proton-transfer spectroscopy beyond the normal-mode scenario," J. Chem. Phys. **157**, 174116 (2022).
[31]R. Zwanzig, "Memory effects in irreversible thermodynamics," Phys. Rev. **124**, 983 (1961).
[32]H. Mori, "Transport, collective motion, and brownian motion," Prog. Theor. Phys. **33**, 423 (1965).
[33]J. E. Straub, M. Borkovec, and B. J. Berne, "Calculation of dynamic friction on intramolecular degrees of freedom," J. Phys. Chem. **91**, 4995 (1987).
[34]C. Uchiyama and F. Shibata, "Unified projection operator formalism in nonequilibrium statistical mechanics," Phys. Rev. E **60**, 2636–2650 (1999).
[35]T. Kinjo and S. Hyodo, "Equation of motion for coarse-grained simulation based on microscopic description," Phys. Rev. E **75**, 051109 (2007).
[36]J. R. Silbermann, M. Schoen, and S. H. L. Klapp, "Coarse-grained single-particle dynamics in two-dimensional solids and liquids," Phys. Rev. E **78**, 011201 (2008).
[37]A. Carof, R. Vuilleumier, and B. Rotenberg, "Two algorithms to compute projected correlation functions in molecular dynamics simulations," J. Chem. Phys. **140**, 124103 (2014).
[38]Z. Li, X. Bian, X. Li, and G. E. Karniadakis, "Incorporation of memory effects in coarse-grained modeling via the Mori-Zwanzig formalism," J. Chem. Phys. **143**, 243128 (2015).
[39]M. te Vrugt and R. Wittkowski, "Mori-Zwanzig projection operator formalism for far-from-equilibrium systems with time-dependent Hamiltonians," Phys. Rev. E **99**, 062118 (2019).
[40]S. Izvekov, "Mori-Zwanzig projection operator formalism: Particle-based coarse-grained dynamics of open classical systems far from equilibrium," Phys. Rev. E **104**, 024121 (2021).
[41]C. Ayaz, L. Scalfi, B. A. Dalton, and R. R. Netz, "Generalized Langevin equation with a nonlinear potential of mean force and nonlinear memory friction from a hybrid projection scheme," Phys. Rev. E **105**, 054138 (2022).
[42]H. Vroylandt and P. Monmarché, "Position-dependent memory kernel in generalized Langevin equations: Theory and numerical estimation," J. Chem. Phys. **156**, 244105 (2022).
[43]H. Vroylandt, "On the derivation of the generalized Langevin equation and the fluctuation-dissipation theorem," Europhys. Lett. **140**, 62003 (2022).
[44]F. N. Brünig, O. Geburtig, A. v. Canal, J. Kappler, and R. R. Netz, "Time-dependent friction effects on vibrational infrared frequencies and line shapes of liquid water," J. Phys. Chem. B **126**, 1579 (2022).
[45]B. A. Dalton, H. Kiefer, and R. R. Netz, "The role of memory-dependent friction and solvent viscosity in isomerization kinetics in viscogenic media," Nat. Commun. **15**, 3761 (2024).
[46]F. N. Brünig, J. O. Daldrop, and R. R. Netz, "Pair-reaction dynamics in water: Competition of memory, potential shape, and inertial effects," J. Phys. Chem. B **126**, 10295 (2022).
[47]Q. Zhou, R. R. Netz, and B. A. Dalton, "Rapid state-recrossing kinetics in non-Markovian systems," arXiv:2403.06604 (2024).
[48]L. Lavacchi, J. O. Daldrop, and R. R. Netz, "Non-Arrhenius barrier crossing dynamics of non-equilibrium non-Markovian systems," Europhys. Lett. **139**, 51001 (2022).
[49]R. Dutta and E. Pollak, "Microscopic origin of diffusive dynamics in the context of transition path time distributions for protein folding and unfolding," Phys. Chem. Chem. Phys. **24**, 25373 (2022).